Supplementary Material

Development of an Axial Cyclone for High-performance: Application of Cycloid Curve and Multi Objective Optimization

Jinill Cho[1], Junho Yun[1] and Taesung Kim[1, 2, *]

[1] Department of Mechanical Engineering, Sungkyunkwan University, Suwon-si, Gyeonggi-do, 16419, South Korea
[2] SKKU Advanced Institute of Nano Technology (SAINT), Sungkyunkwan University, Suwon-si, Gyeonggi-do, 16419, South Korea
[†] These authors contributed equally to this work

1. Numerical methods

1.1 Turbulent model

A typical cyclone separator has a unique gas motion, exhibiting a high swirling number and intense vorticity in anisotropic turbulence. Selecting an appropriate turbulence model plays a pivotal role in predicting turbulent flows with high swirl. To simulate the flow field inside a cyclone, several researchers have investigated the use of favorable turbulent models such as the Reynolds-stress model because of their high accuracy (Hoekstra, Derksen, & Van Den Akker, 1999; Veerapen, Lowry, & Couturier, 2005). This model was combined and adapted in this flow simulation to handle the challenging situation of anisotropic turbulent two-phase flow in the dispersed phase (Huang, 2005). Owing to this suitability for strong anisotropy from high swirling and streamline curvature, Reynolds-stress model has been widely used to predicts cylcone's performance (Kaya, Fuat, and I. Karagoz, 2008). Furthermore, the turbulence model generally takes less computer capacity and requires shorter computing time than large eddy simulation does due to the large requirement on the mesh (Slack et al., 2000). Therefore, it was selected in this study as the turbulent model. Based on the Reynolds stress transport equation, the equation can be rewritten as (Babaoğlu, Parvaz, Hosseini, Elsayed, & Ahmadi, 2021):

$$\frac{\partial}{\partial t}R_{ij} + \overline{u_k}\frac{\partial}{\partial x_k}R_{ij} = \frac{\partial}{\partial x_k}\left(\frac{\nu_t}{\sigma^k}\frac{\partial}{\partial x_k}R_{ij}\right) - \left[R_{ik}\frac{\partial \overline{u_j}}{\partial x_k} + R_{jk}\frac{\partial \overline{u_i}}{\partial x_k}\right] - C_1\frac{\varepsilon}{K}\left[R_{ij} - \frac{2}{3}\delta_{ij}K\right] - C_2[P_{ij} - \frac{2}{3}\delta_{ij}P] + -\frac{2}{3}\delta_{ij}\varepsilon, \quad (1)$$

where P_{ij} is the turbulence production term and is defined as follows:

$$P_{ij} = -\left[R_{ik}\frac{\partial \overline{u_j}}{\partial x_k} + R_{jk}\frac{\partial \overline{u_i}}{\partial x_k}\right] \quad (2)$$

$$P = \frac{1}{2} P_{ii} \tag{3}$$

where P is the turbulence kinetic energy production and ν_t is the turbulent eddy viscosity. The value of σ^k in the turbulent diffusive transport term was set as 1. The values of C_1 and C_2 in the pressure strain term are defined as 1.8 and 0.60 in Ansys fluent 2020 R2.

1.2 Discrete phase model

Discrete phase modeling (DPM) was employed to verify the particle trajectory and calculate the separation efficiency. The DPM for simulating multiphase flow is based on the Eulerian-Lagrangian method. The method operates under the assumption that the gas phase is regarded as a continuum field, whereas the discrete phase is tracked by the Lagrangian particle trajectory (Safikhani, Zamani, & Musa, 2018). The following equation expresses the balance of forces exerted on a particle due to the fluid force.

$$m_p \frac{d\vec{u}_p}{dt} = m_p \frac{\vec{u}-\vec{u}_p}{\tau_r} + m_p \frac{\vec{g}(\rho_p-\rho)}{\rho_p} + \vec{F}, \tag{4}$$

where m_p is the particle mass, $\vec{u}$ is the fluid phase velocity, $\vec{u}_p$ is the particle velocity, ρ is the fluid density, ρ_p is the density of the particle, $\vec{F}$ is an additional force, $m_p \frac{\vec{u}-\vec{u}_p}{\tau_r}$ is the drag force, and τ_r is the droplet or particle relaxation time, which is defined as

$$\tau_r = \frac{\rho_p d_p^2}{18\mu} \frac{24}{C_d Re}, \tag{5}$$

where μ is the molecular viscosity of the fluid, C_d is the drag coefficient, d_p is the particle diameter, and Re is the relative Reynolds number, which is defined as

$$Re \equiv \frac{\rho d_p |\vec{u}_p - \vec{u}|}{\mu} \tag{6}$$

Turbulent dispersion by the Discrete Random Walk model were adopted for the trajectories of the injected particles. The interactions and collisions between particles are assumed to be negligible owing to the low volume fraction caused by the low particle concentration. Using DPM model allows for reliable predictability given that the volume fraction of particles is less than 10% of the gas phase. In addition, the reflection coefficient of the walls is defined as 1.0, assuming perfectly elastic collisions. The density of the particles was set to 2000 kg/m^2, and they were injected at the inlet surface at the same velocity as the air flow. The shape of the dispersed particles is assumed to be totally spherical; therefore, the injected total mass flow rate is 0.08 kg/s. The applied particle size distribution ranged from 1.0 − 100 μm using the Rosin Rammler method (Fluent, 2012).

$$Y_d = e^{-(d/\bar{d})^n}, \tag{7}$$

where $\bar{d}$ is the mean diameter and n is the spread parameter. The values of $\bar{d}$ and n in the equation were defined as 50 μm and 3.5, respectively.

1.3 Swirl number

The swirl number typically defines the degree of swirl for swirling flows and was originally defined by Chigier and Beer (Chigier and Beer, 1964). For this study, the simplified equation proposed by Sheen et al. (Sheen et al., 1996) was used, and the equation can be expressed as

$$S_n = \frac{G_t}{RG_{ax}} = \frac{\int_0^R UWr^2 dr}{R\int_0^R U^2 r dr}, \quad (8)$$

where G_t is the axial flux of the tangential momentum, G_{ax} is the axial flux of the axial momentum, R is the raidal position, *and* U and W are the axial and tangential velocity, respectively, at the corresponding radial radius position r.

1.4 Solver settings and boundary conditions

The computational simulation methods used the semi-implicit method pressure-linked equations consistent (SIMPLEC) algorithm to couple the pressure and velocity. Furthermore, PRESTO! (pressure staggering option) was used to apply discretization with high pressure and momentum. The momentum, turbulent kinetic energy, turbulent dissipation rate, and Reynolds stress terms were computed using a second-order upwind scheme for higher-order accuracy. The scaled residuals for all terms were set to less than 10^{-6} as convergence criteria. The wall adopted a no-slip condition as well as the standard wall function to handle the interaction with fluid near wall. Two outlets were set for the pressure outlet: one surface outward and the other with its surface toward a dust box. The outlet of the vortex finder was adopted as the “Escape” boundary condition and the outlet of the dust box was adopted as the “Trap” for recording the number of separated particles. The outlet

1.5 Response surface method

RSM aims to statistically analyze the functional relationship between two variables X and Y by rendering a three-dimensional surface in response to two variables to find the optimal point. The second-order model has been used as a prevailing mathematical model for approximating functions with variables when the response trend has a curved surface. It can be expressed as (Montgomery, 2017)

$$y = \beta_0 + \sum_{i=1}^{k} \beta_i x_i + \sum_{i=1}^{k} \beta_{ii} x_i^2 + \sum_i \sum_{<j} \beta_{ij} x_i x_j + \varepsilon \quad (9)$$

where y denotes the response variable as a function of x_i and x_j input variables, and β_o, β_i, β_{ii}, and β_{ij} are regression coefficients in terms of intercept, linear, quadratic, and interaction, respectively. In addition, ε represents experimental error.

Table S1. Grid independence test for the OO model, CO model, CC model, and OC model.

Original guiding vane + original guiding cone (OO model)		
Number of elements	Pressure drops (Pa)	Relative percentage difference (%)
1,354,621	950.5	2.51
2,014,561	932.1	1.94
4,001,421	925.2	0.74
8,214,621	923.4	0.19
Cycloid guiding vane + original guiding cone (CO model)		
Number of elements	Pressure drops (Pa)	Relative percentage difference (%)
1,217,583	1215.2	2.44
1,817,312	1200.2	1.24
3,981,872	1195.4	0.40
7,214,991	1193.7	0.14
Cycloid guiding vane + cycloid guiding cone (CC model)		
Number of elements	Pressure drops (Pa)	Relative percentage difference (%)
1,264,845	1078.5	3.80
1,896,345	1061.1	1.61
4,054,123	1056.7	0.41
8,465,211	1055.7	0.09
Original guiding vane + cycloid guiding cone (OC model)		
Number of elements	Pressure drops (Pa)	Relative percentage difference (%)
1,154,324	801.1	2.90
2,504,156	791.6	1.19
4,124,578	787.2	0.56
8,132,456	786.1	0.14

Table S2. The nomenclature, project, and values of experimental design.

Nomenclature	Component	Values [m] or [degree]
A_1	Guiding cone rear length	0.017
A_2	Guiding cone length	0.023
A_3	Vane part length	0.048
P_1	Cone and outlet distance	0.013
P_2	Outlet inner diameter	0.04
P_3	Outlet protrusion length	0.024
P_4	Collection outer diameter	0.018
D_1	Inlet diameter	0.063
D_2	Outlet outer diameter	0.042
Θ	Guiding cone rear degree	8

Table S3. Design of points from Latin Hypercube sampling.

No.	Input parameter [m]				Output parameter	
	P1	**P2**	**P3**	**P4**	$\boldsymbol{\eta}$	$\boldsymbol{\Delta p}$
1	0.225	0.0484	0.0224	0.0192	72.04336	1109.949
2	0.249	0.054	0.0264	0.0184	61.8736	1105.689
3	0.153	0.05	0.0328	0.0136	65.20165	1186.173
4	0.237	0.0588	0.0216	0.0176	99.60411	1104.306
5	0.165	0.0436	0.0304	0.0256	72.04336	1099.838
6	0.291	0.0524	0.0288	0.0272	72.04336	1046.376
7	0.231	0.0548	0.028	0.0264	99.71366	1071.483
8	0.285	0.0452	0.0332	0.02	72.04336	1092.926
9	0.195	0.0556	0.032	0.024	66.87516	1100.189
10	0.183	0.0444	0.0192	0.0296	55.8395	1083.744
11	0.207	0.042	0.0208	0.0112	72.04336	1169.157
12	0.177	0.058	0.0184	0.0208	55.31019	1122.934
13	0.219	0.0572	0.0336	0.016	64.18568	1123.04
14	0.255	0.0476	0.0344	0.012	72.04336	1144.519
15	0.201	0.0596	0.0272	0.028	96.96672	1064.031
16	0.273	0.0468	0.0196	0.0168	53.30062	1115.109
17	0.267	0.046	0.0368	0.0288	100	1044.809
18	0.243	0.0508	0.036	0.0128	72.04336	1159.134
19	0.171	0.0412	0.0352	0.0144	72.04336	1177.564
20	0.159	0.0532	0.0276	0.0152	99.78132	1189.438
21	0.213	0.0516	0.0248	0.0248	66.94136	1093.263
22	0.279	0.0564	0.024	0.0104	72.04336	1118.002
23	0.297	0.0492	0.0212	0.0216	65.09692	1086.218
24	0.189	0.0428	0.0256	0.0232	72.04336	1093.806
25	0.261	0.0404	0.031	0.0224	72.04336	1097.286

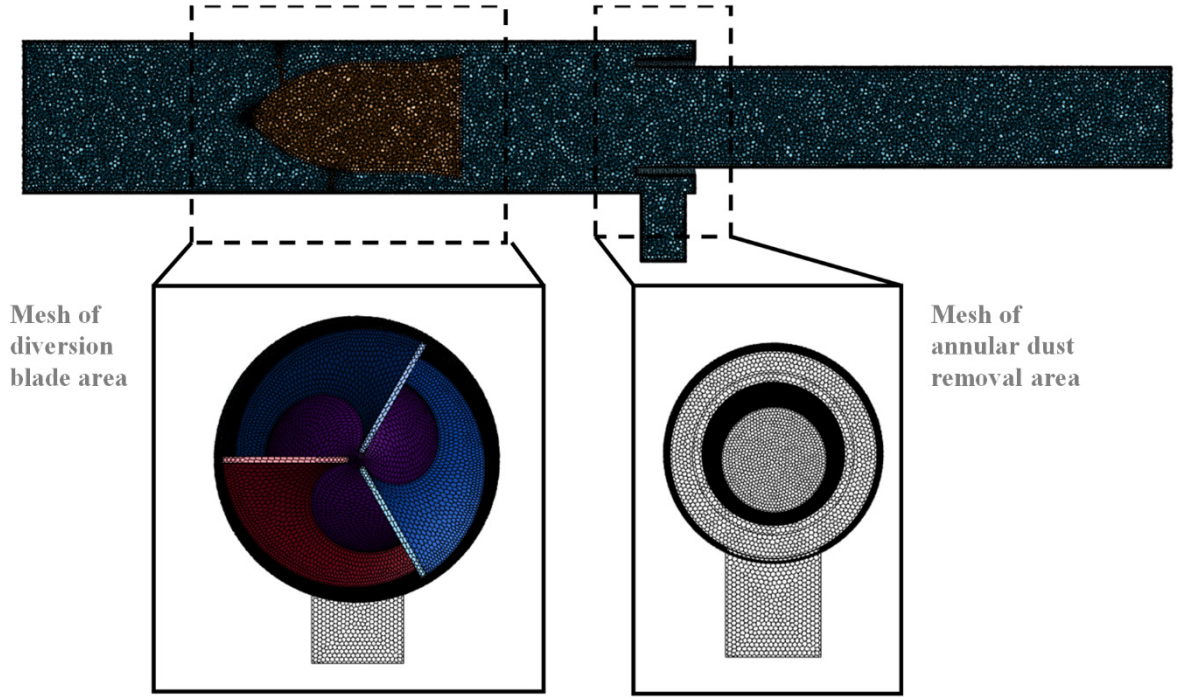

Fig. S1. A polyhedral shape mesh for numerical simulation.

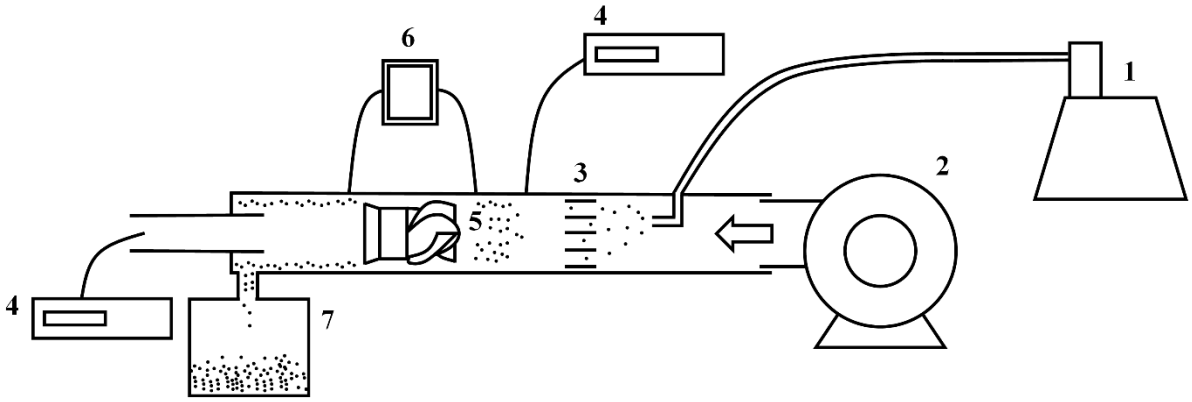

Fig. S2. Schematic of the system. (1) dust generator, (2) main blower, (3) honeycomb, (4) dust monitors, (5) cyclone, (6) differential pressure gauge, and (7) dust box.

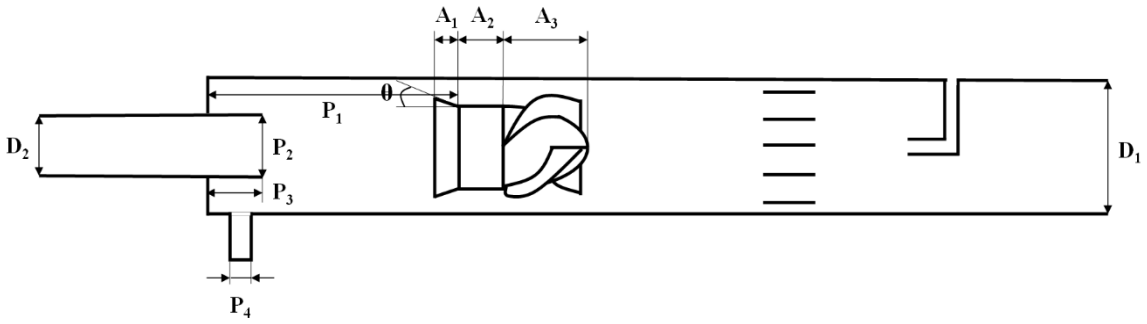

Fig. S3. The configuration of the separation system.

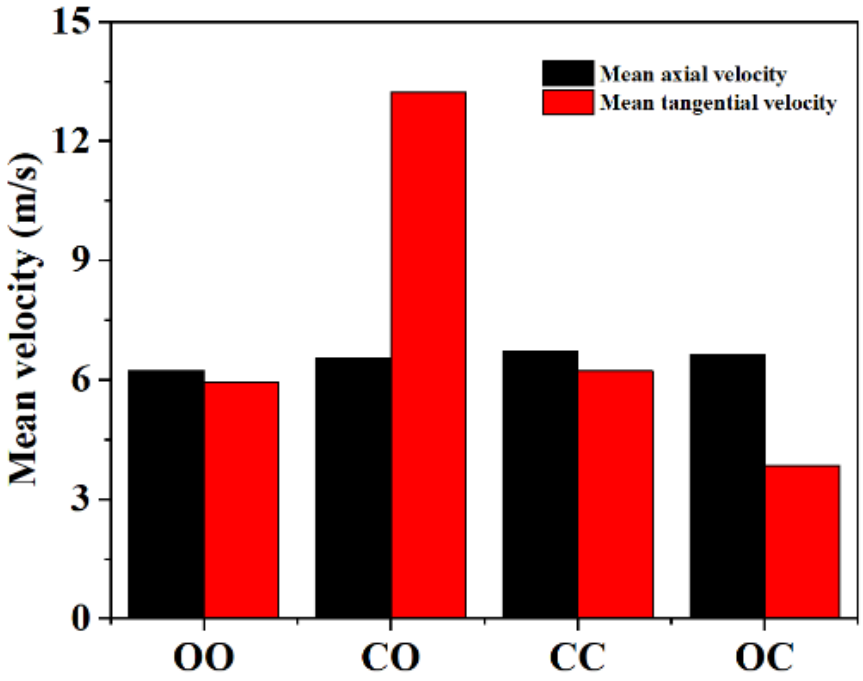

Fig. S4. Mean axial and tangential velocity on an area of the OO model, CO model, CC model, and OC model

REFERENCES

Babaoğlu, N. U., Parvaz, F., Hosseini, S. H., Elsayed, K., & Ahmadi, G. (2021). Influence of the inlet cross-sectional shape on the performance of a multi-inlet gas cyclone. Powder Technol 384, 82-99. https://doi.org/10.1016/j.powtec.2021.02.008

Chigier, N. A., & Bee´ r, J. M. (1964). Velocity and static-pressure distributions in swirling air jets issuing from annular and divergent nozzles. J. Fluids Eng 86(4), 788-796. https://doi.org/10.1115/1.3655954

Kaya, F., & Karagoz, I. (2008). Performance analysis of numerical schemes in highly swirling turbulent flows in cyclones. Curr. Sci. 94(10), 1273-1278. http://www.jstor.org/stable/24100235

Fluent, A. (2012). 14.5, theory guide. Canonsburg, PA: ANSYS: Inc.

Hoekstra, A. J., Derksen, J. J., & Van Den Akker, H. E. A. (1999). An experimental and numerical study of turbulent swirling flow in gas cyclones. Chem. Eng. Sci. 54(13-14), 2055-2065. https://doi.org/10.1016/S0009-2509(98)00373-X

Huang, S. (2005). Numerical simulation of oil-water hydrocyclone using reynolds-stress model for eulerian multiphase flows. Can. J. Chem. Eng 83(5), 829-834. https://doi.org/10.1002/cjce.5450830504

Slack, M.D., Prasad, R.O., Bakker, A., & Boysan, F. (2000). Advances in cyclone modelling using unstructured grids. Chem. Eng. Res. Des. 8(78), 1098-1104. https://doi.org/10.1205/026387600528373

Sheen, H. J., Chen, W. J., Jeng, S. Y., & Huang, T. L. (1996). Correlation of swirl number for a radial-type swirl generator. Experimental thermal and fluid science, 12(4), 444-451. https://doi.org/10.1016/0894-1777(95)00135-2

Safikhani, H., Zamani, J., & Musa, M. (2018). Numerical study of flow field in new design cyclone separators with one, two and three tangential inlets. Adv. Powder Technol. 29(3), 611-622. https://doi.org/10.1016/j.apt.2017.12.002

Veerapen, J. P., Lowry, B. J., & Couturier, M. F. (2005). Design methodology for the swirl separator. Aquac. Eng. 33(1), 21-45. https://doi.org/10.1016/j.aquaeng.2004.11.001